Available online at www.sciencedirect.com
SCIENCE DIRECT®
Composites Science and Technology 65 (2005) 537–549
COMPOSITES SCIENCE AND TECHNOLOGY
www.elsevier.com/locate/compscitech

Use of a cohesive-zone model to analyze the fracture of a fiber-reinforced polymer–matrix composite

S. Li [a], M.D. Thouless [a,b,*], A.M. Waas [c], J.A. Schroeder [d], P.D. Zavattieri [d]

[a] Department of Mechanical Engineering, University of Michigan, Ann Arbor, MI, USA
[b] Department of Materials Science and Engineering, University of Michigan, 2282, G.G. Brown Building, Ann Arbor, MI 48109-2125, USA
[c] Department of Aerospace Engineering, University of Michigan, Ann Arbor, MI, USA
[d] R&D Planning, General Motors, Warren, MI, USA

Received 18 February 2004; received in revised form 12 July 2004; accepted 23 August 2004

Abstract

A cohesive-zone model for a fiber-reinforced polymer–matrix composite is presented. A two-parameter model with a characteristic toughness and a characteristic strength can be used to predict the fracture of notched or cracked specimens. The two parameters can be determined by comparing numerical predictions to experimental observations of a fracture test. It is shown that the engineering behavior, in terms of strength, deformation and energy dissipation is well-described by such a two-parameter model, but when the characteristic dimensions of the composite structure (e.g., the initial crack length or ligament length) are very small, extra details about the cohesive law such as the matrix-cracking strength may be required. Finally, it is shown that a cohesive-zone model provides excellent predictions of transitions between stable and catastrophic crack growth in the composite, and, hence, permits an understanding of the energy dissipation during fracture that occurs in these different regimes.

Keywords: B. Fracture; Composite

1. Introduction

Over the last few decades there has been much interest in developing failure criteria for laminated polymer–matrix composites used in aerospace applications [16]. A major focus has been on understanding the mechanics of delamination [36–38]. In recent years, there has been renewed interest in the properties of monolithic polymer–matrix composites for automotive applications. The fundamental physics that governs crack propagation in these materials is based on the original insights of Marshall et al. [3], and was put into a fracture-mechanics framework by Aveston et al. [31]. An effective brittle-matrix composite reinforced by strong brittle fibers relies on the fibers being only weakly bonded to the matrix. When a crack passes through the matrix it leaves a wake of intact fibers behind the tip. These fibers exert closing tractions on the crack surface and, as the fibers pull-out of the matrix, they do work against frictional forces at the matrix–fiber interface. This work dissipates energy and contributes to the toughness of the composite.

Models for fracture of brittle-matrix composites are generally based on a fracture-mechanics approach, with the notion that a sharp crack propagates into the matrix with bridging fibers behind the tip [31]. The matrix crack is assumed to propagate when the energy-release rate acting at the crack tip is equal $(1-c_f)\Gamma_m$, where Γ_m is the matrix toughness and c_f is the area fraction of fibers on the crack plane. The role of the bridging fibers is to reduce the energy-release rate available to propagate the matrix crack. If an initially unbridged crack exists in the composite (Fig. 1(a)), it will begin to propagate into the matrix when the applied energy-release rate

* Corresponding author. Tel.: +1 734 763 5289; fax: +1 734 647 3170.
E-mail address: thouless@engin.umich.edu (M.D. Thouless).

0266-3538/$ - see front matter © 2004 Elsevier Ltd. All rights reserved.
doi:10.1016/j.compscitech.2004.08.004

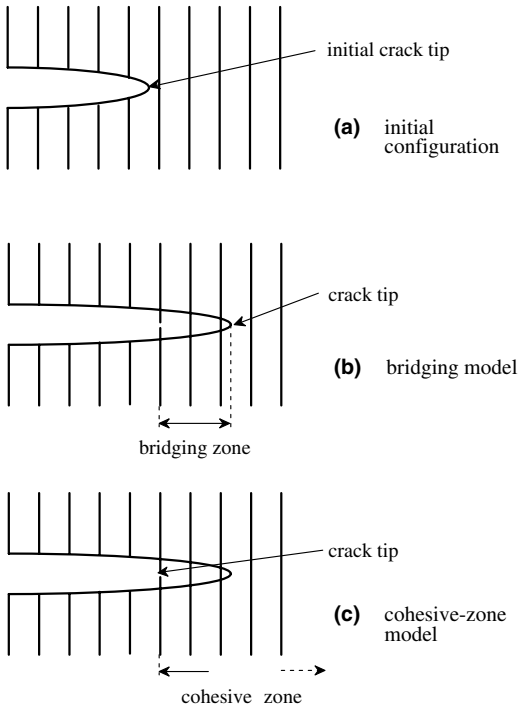

Fig. 1. (a) An initially unbridged crack in a fiber-reinforced composite. (b) A bridging-model view of a crack advancing into the matrix, leaving a wake of bridging fibers behind the tip. (c) A cohesive-zone view of the same crack with a cohesive zone advancing into the matrix ahead of the crack tip.

equals $(1-c_f)\Gamma_m$. As the crack extends, it leaves a wake of bridging fibers behind its tip (Fig. 1(b)). The tractions exerted by these fibers do work and dissipate energy, increasing the applied energy-release rate required to continue propagating the crack. This results in *R*-curve behavior, with the apparent toughness of the crack increasing with crack length. Eventually, the opening of the crack is sufficient to pull the fibers completely out of the matrix (or the load supported by the fibers is sufficient to cause them to fail), and the steady-state limit of toughness is reached. The increment of toughening associated with bridging by the fibers is given by [7]:

$$\Gamma_b = \int_0^{\delta_c} \sigma \, d\delta, \tag{1a}$$

where σ is the average stress exerted on the crack by the fibers, δ is the effective opening of the crack (accounting for the relative slip between fibers and matrix [44]), and δ_c is the critical crack opening at which the tractions go to zero. Ignoring any contribution of fiber fracture to the toughness, the total steady-state toughness of the composite is then given by

$$\Gamma = (1 - c_f\phi)\Gamma_m + \Gamma_b. \tag{1b}$$

Micromechanics models focus on deriving expressions for the relationship between the tractions and the crack opening. For frictional sliding these generally result in a relationship of the form $\sigma \propto \delta^{1/2}$ [31]; other modifications include the effects of variable fiber strengths [14,45] and inclined fibers [18,26]. These relationships can then be incorporated into fracture mechanics analyses to understand the behavior of bridged cracks [9,31,32,35]. The bridging law can also be determined experimentally. Li and co-workers [23,25,27] did this for a cement–matrix composite by relating the measured *J*-integral [34] to the opening displacement of the tip of the initial crack. A similar approach was adopted in studies of epoxy–matrix composites [28,39,40]. Alternative approaches for deducing the bridging law include backing out the tractions from observed crack-tip profiles [12,30], or measuring the law directly from fully cracked but bridged tensile specimens [10].

Once the bridging law is known, the fracture behavior of the composites can be modeled, and phenomena such as notch-sensitivity [8,10,11,29,42] and ductile-to-brittle transitions [4,8,13,24] can be analyzed. Two important parameters that describe fiber bridging behind the crack tip are the steady-state toughness, Γ_b, and a characteristic strength, $\hat{\sigma}_b$, (or, a characteristic crack-opening displacement). A characteristic fracture length scale is given by the parametric group $E\Gamma_b/\hat{\sigma}_b^2$, where E is the modulus of the composite. If this quantity is significantly smaller than all of the characteristic geometrical length scales (such as crack length or notch size), then the composite behaves in a notch- or crack-sensitive fashion [42]. Conversely, the composite is considered to be "notch" or "crack insensitive" (or "notch ductile") when $E\Gamma_b/\hat{\sigma}_b^2$ is large compared to any of the characteristic geometrical length scales.

An alternative approach to analyzing fracture is provided by cohesive-zone models, as they have evolved from the early work by Dugdale [15] and others [5,6]. An essential feature of these models that distinguish them from bridged-crack models is that they automatically introduce a strength-based fracture criterion [1] (cohesive strength) in conjunction with an energy-based fracture criterion (toughness) for the material *ahead of the crack tip*. Fracture analyses are done by embedding cohesive-zone elements along the fracture plane that deform according to a traction–separation law having the appropriate strength and toughness (area under the traction–separation curve) [33,46,47]. Generally, cohesive-zone models (also known as damage models) and bridged-crack models can be considered to be merely different perspectives of the same phenomenon, with the difference between them being what is regarded to be the crack tip [43]. In a cohesive-zone model both the crack-fiber interaction and the matrix cracking is associated with damage *ahead* of a crack tip (Fig. 1(c)), which is characterized by the steady-state toughness, Γ, and a characteristic strength, $\hat{\sigma}$ associated with

[1] Or, equivalently, a displacement-based fracture criterion.

this toughness. The strength parameter can be neglected if the fracture length scale, $E\Gamma/\hat{\sigma}^2$, is significantly smaller than any characteristic geometrical length scale such as the crack size. The usual analyses of linear-elastic fracture mechanics. are then appropriate, and the toughness parameter alone can be used to describe crack propagation.

In such a simple two-parameter form of the cohesive-zone model, no distinction is made between matrix-cracking and fiber-bridging. If a distinction between these two phenomena is required, the traction–separation law can be broken up into two components – one associated with matrix cracking and one with fiber bridging. A schematic illustration of such a law is shown in Fig. 2, where a second characteristic strength, in the form of a matrix-cracking strength, $\hat{\sigma}_m$, is introduced into the problem. If the matrix toughness, Γ_m, makes a small contribution to the total toughness (i.e., $\Gamma \approx \Gamma_b$), then the characteristic strength of the cohesive region is equal to $\hat{\sigma}_b$, and the matrix-cracking strength can generally be ignored. Conversely, if Γ is dominated by the matrix toughness, and the bridging contribution can be ignored, then the characteristic strength of the cohesive-zone model is equal to $\hat{\sigma}_m$, and $\hat{\sigma}_b$ can be ignored.

An ability to deduce fracture properties for a composite, and then to predict the behavior when the composite is bonded or loaded in different geometries is very important for design. It is the development of such quantitative design tools that motivated the present work, of which this paper is the first step in the process. It is assumed that the intent of such design tools is to predict the performance of a composite from an engineering perspective: i.e., to predict macroscopic strengths and deformations of different geometries. Generally, details of the cohesive law do not affect calculations for crack propagation – often only the characteristic strength and toughness parameters are important. [2] Furthermore, cohesive-zone models can be easily implemented numerically for the efficient analysis of arbitrary geometries. As has been demonstrated for adhesive joints [48,49], two-parameter cohesive-zone models provide a very powerful tool for predicting fracture.

In the present paper, the use of a mode-I cohesive-zone model and the determination of the appropriate parameters is investigated for a polypropylene/glass-fiber composite. First, the constitutive properties of the composite were determined by tensile and shear tests, then compact-tension specimens were used to determine the mode-I cohesive parameters for the composite by comparing experimental results to numerical predictions for crack propagation. A comparison of these parameters to tensile tests of uncracked specimens suggested that a second strength parameter was required under some circumstances for this particular material. This introduced the need to distinguish between a characteristic strength (associated with the dominant toughening mechanism) and a cohesive strength in a cohesive-zone model. Finally, the predictive capability of the cohesive-zone model was verified by examining the behavior of single edge-notched tensile specimens. It was shown how fracture instabilities could be predicted accurately. A companion paper discusses the incorporation of the cohesive-zone model developed for this composite into a model for adhesively bonded joints [21]. Ongoing work is extending these concepts into mixed-mode failure [22].

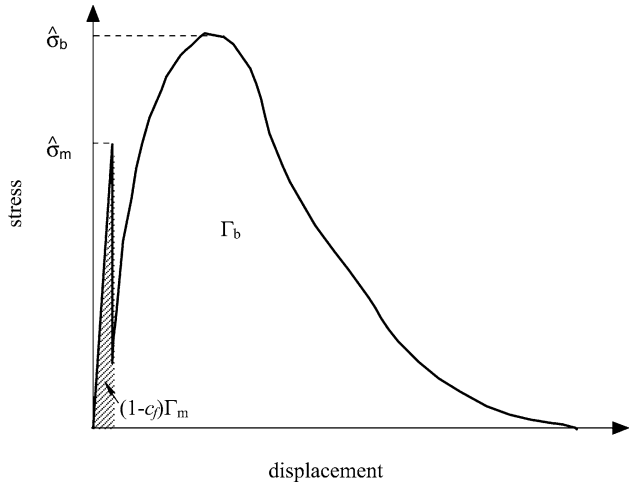

Fig. 2. A schematic traction–separation law that could be used to link cohesive-zone models and bridged-crack models of crack growth, by separately identifying the phenomena of matrix-cracking and fiber-bridging.

2. Characterization of the materials used in this study

The composite used in this study was a polypropylene-based thermoplastic composite reinforced with 19% (by volume) glass fibers, in the form of a randomly oriented mat. [3] According to the specifications provided by the manufacturer, the diameter of the glass fibers was about 23.5 μm, with 97% of the glass fibers being nominally "continuous", and the rest having a length of less than about 6 mm. The composite was received in plaque form; it was re-molded to consolidate the material and to obtain plaques of different thicknesses. This was done by pre-heating the as-received material at 210 °C for 10 min, and then re-molding it using a hydraulic press at 70 °C and 13 MPa for about 1.5 min. Micrographs of sections of the re-molded composite are shown in Fig. 3. The constitutive properties of the composite were

[2] Bridging analyses often rely on calculating the stress-intensity factor acting at the matrix crack tip, so that details of the bridging law may affect the results.

[3] Azdel R401 provided by Azdel, Inc.

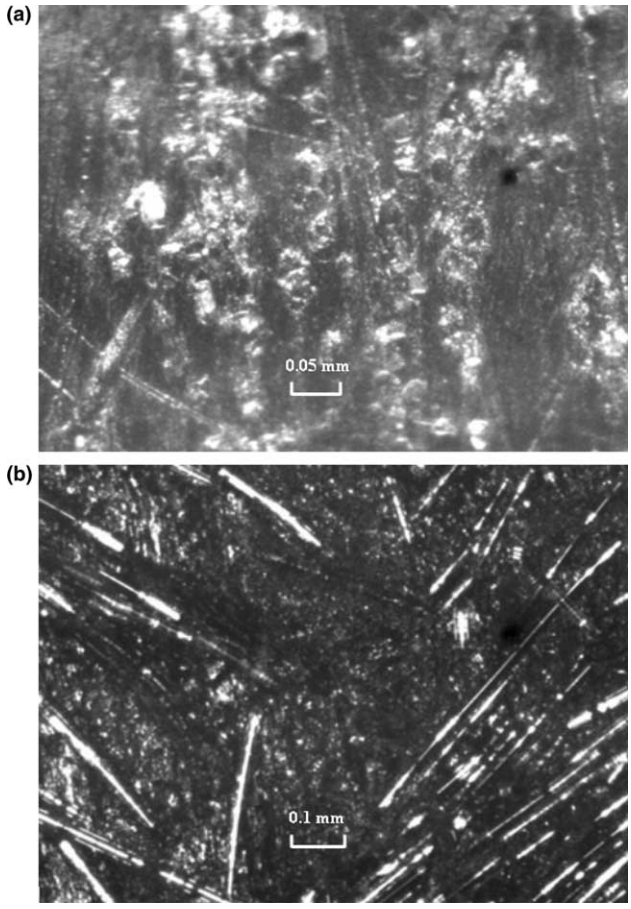

Fig. 3. Micrographs of polished sections of the composite: (a) perpendicular to the fiber mat and (b) parallel to the fiber mat.

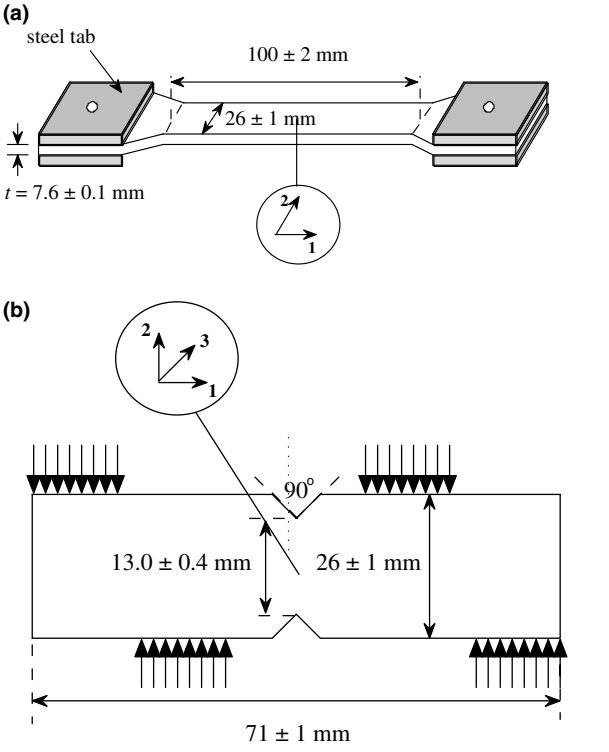

Fig. 4. (a) Geometry of specimens used for the tensile tests. Strain gauges were mounted in the one and two directions. (b) Geometry of specimens used for Iosipescu shear tests. Strain gauges were mounted in the one, two and three directions. The out-of-plane thickness for both sets of tests was $t = 7.6 \pm 0.1$ mm.

characterized by performing uniaxial tensile tests (Fig. 4(a)) and Iosipescu shear tests (Fig. 4(b)) [2] on specimens cut from orthogonal directions. No significant difference in the behavior was observed between the two different orientations, suggesting that the composite properties could be treated as being transversely isotropic. The tensile tests, performed at a displacement rate of 0.76 mm/min, indicated that the composite deformed in an essentially elastic fashion with a tensile strength of 100 ± 20 MPa (Fig. 5(a)). Although this elastic deformation was not completely linear, it could, within the range of variability of the properties of the composite, be modeled by a tensile modulus of 6.0 ± 1.5 GPa, and a Poisson's ratio of 0.30 ± 0.03. Since this range of elastic properties could be obtained from specimens cut from a single plaque of the composite, it appeared that the properties of the composite were not very homogeneous. At failure, a single crack propagated across the specimen and, although there was extensive fiber pull-out on the fracture surface, the failure was catastrophic in the sense that the load dropped immediately to zero with no indication of crack growth before the drop (i.e., there was no quasi-static crack growth: a transition to dynamic fracture occurred immediately). There were no visible edge flaws in the samples, and polishing did not affect this behavior. Conversely, the shear tests performed at a displacement rate of 0.2 mm/min indicated elastic/perfectly plastic behavior with a shear yield strength of 65 ± 15 MPa (Fig. 5(b)). [4] The in-plane shear modulus was determined to be 2.3 ± 0.5 GPa, which is consistent with the in-plane elastic constants derived from the tensile tests (again, confirming the transversely isotropic nature of the composite).

3. Determination of mode-I cohesive parameters

The cohesive parameters of the composite were determined by means of compact-tension specimens with the dimensions shown in Fig. 6. The load–displacement curves obtained from these specimens at a displacement rate of 0.4 mm/min are illustrated in Fig. 7. No significant difference was observed for specimens machined in orthogonal directions from the plaques.

[4] Despite the possible overlap in the range of uncertainty for the shear yield strength and for the tensile strength, no yield behavior was ever observed in the 20 tensile specimens that were tested.

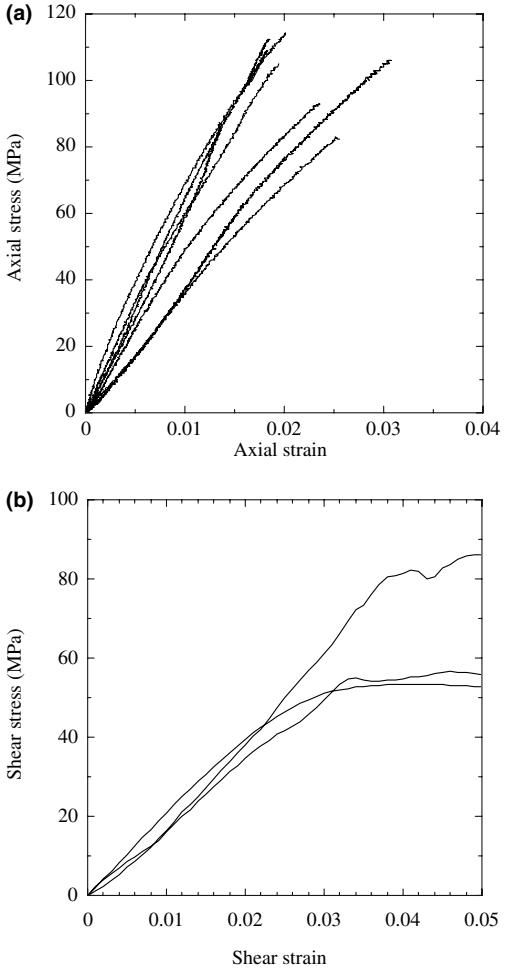

Fig. 5. (a) Normal stress–strain curves from the tensile tests. (b) Shear stress–strain curves from the Iosipescu shear tests. These figures show an example of a characteristic curve, and an indication of the experimental range of data.

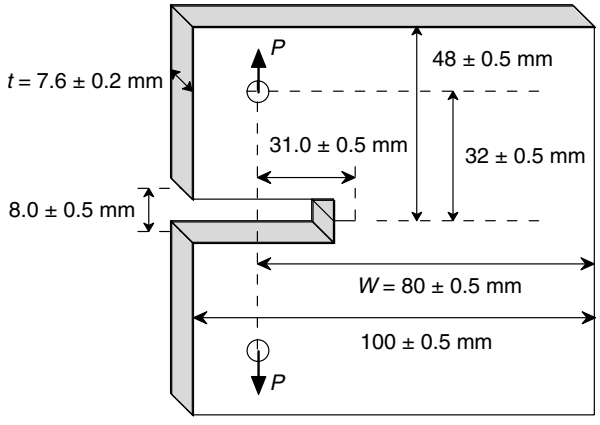

Fig. 6. Geometry for the compact-tension specimens used to investigate the fracture properties of the composite. The displacement was measured at the crack mouth by means of an extensometer. Side grooves with a depth of approximately 0.1–0.2 mm were used to maintain a co-linear crack.

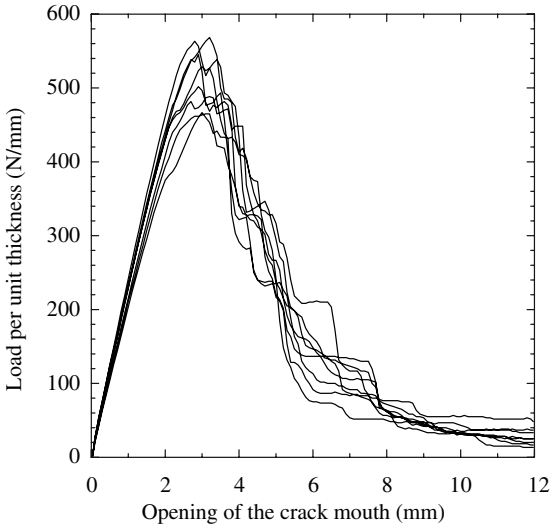

Fig. 7. Plots of the load (per unit thickness) against crack-mouth opening for the compact tension specimens. The modulus for the samples used to produce this plot ranged from between 6.4 and 7.5 GPa.

The compact-tension geometry shares a characteristic with the double-cantilever beam [20] in that the decreasing portions of the load–displacement curves, obtained after the crack begins to grow, are very sensitive indicators of the mode-I toughness, Γ (area under the traction–separation curve), and relatively insensitive to the cohesive strength. Therefore, the toughness was obtained by matching this region of the load–displacement curves to predictions from numerical analyses that incorporated a cohesive zone at the crack tip. Details of the numerical analyses are given in [19]. The calculations were done using the ABAQUS finite-element program (version 6.3), with the bulk composite being modeled by continuum elements with constitutive properties as described earlier. The fracture plane ahead of the crack incorporated four-noded user-defined elements that followed the traction–separation law of Fig. 8. Since numerical simulations had demonstrated that the precise shape of the traction–separation law did not fundamentally affect the results of the analysis, the simple triangular law of Fig. 8 was initially chosen as the simplest one that is completely described by the two dominant cohesive parameters of strength and toughness. The area under the traction–separation law of the cohesive-zone was adjusted until the numerical predictions for the decaying portion of the load–displacement plot matched the experimental results shown in Fig. 7. After the toughness had been determined, the characteristic strength was obtained by varying the maximum stress in the traction–separation law, while maintaining the toughness at a constant value, until the full load–displacement curve could be fitted to the experimental

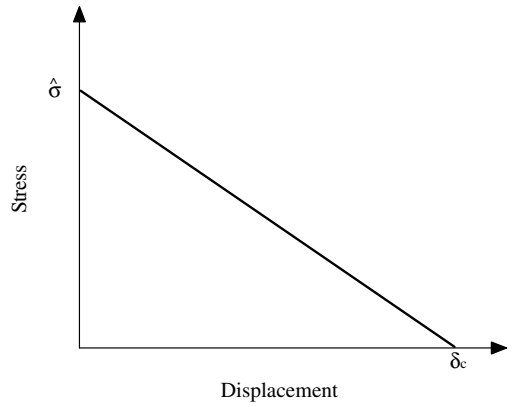

Fig. 8. Schematic illustrations of the linear cohesive law used for the two-parameter cohesive-zone model.

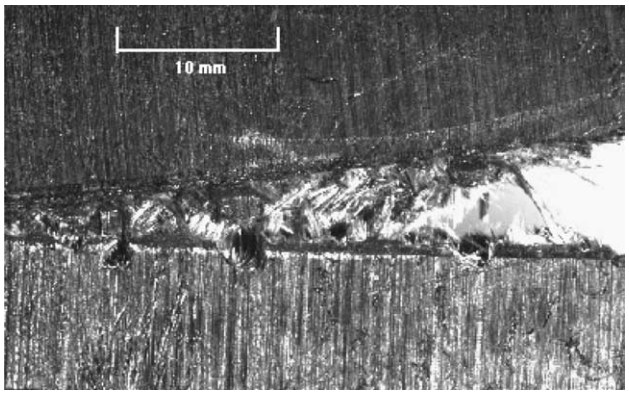

Fig. 10. Micrograph of the crack-tip region in a compact-tension specimen.

data. Since different coupons of the composite exhibited considerable variability in elastic modulus, the cohesive-zone parameters were found by comparing the experimental data to numerical calculations using the appropriate value of modulus for each specimen. The final results of these calculations showed that the mode-I toughness was $\Gamma = 40 \pm 4\ \mathrm{kJ\,m^{-2}}$, and the characteristic strength was $\hat{\sigma} = 79 \pm 8$ MPa.

The resultant predictions for the load–displacement curves are compared to the experimental results in Fig. 9. This figure has been plotted in a normalized fashion to reduce the effect of the modulus variability.

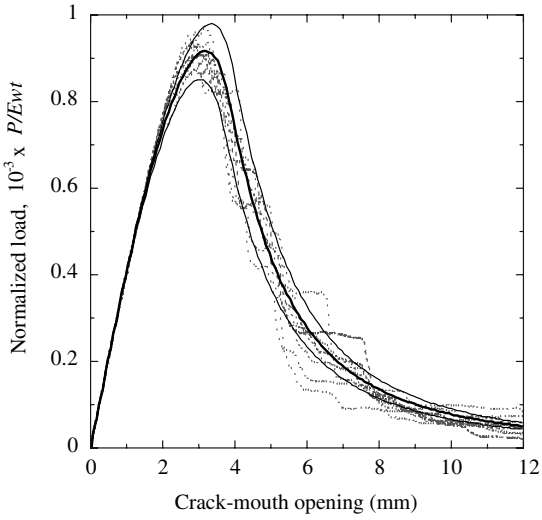

Fig. 9. A plot of normalized load (P/Etw) against the crack-mouth opening for the compact-tension geometry of Fig. 6. This curve shows a comparison between the predictions of a cohesive-zone model and the experimental results. The thicker solid line represents the predictions with fiber-bridging strength of 79 MPa, a toughness of 40 $\mathrm{kJ\,m^{-2}}$, and a modulus of 7.0 GPa. The thinner solid lines represent the range of uncertainty for the calculations for the range of the cohesive parameters quoted in the text, and the modulus of the specimens.

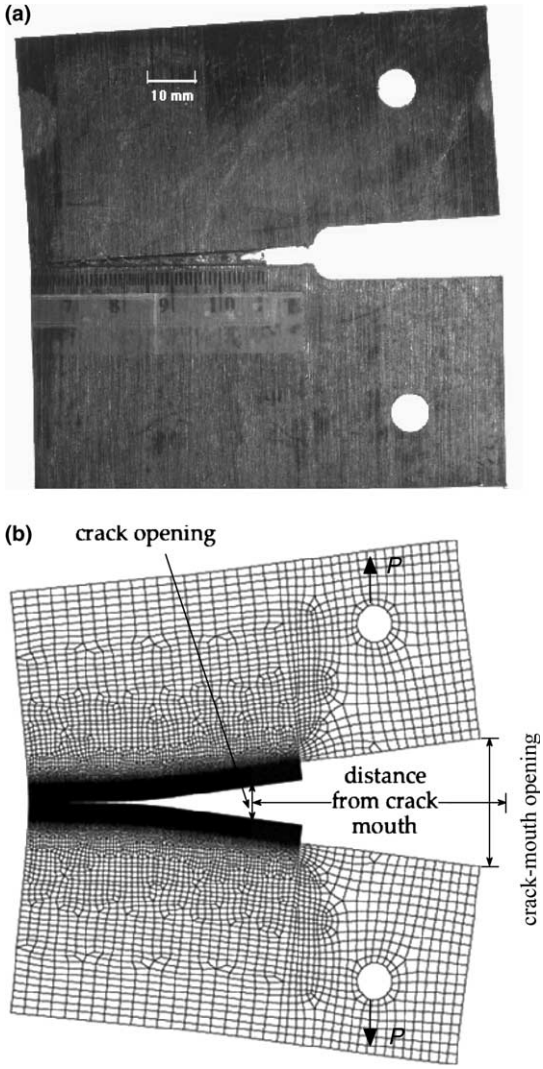

Fig. 11. (a) An optical micrograph of a compact-tension specimen, and (b) a diagram of the finite-element model used to determine displacements ahead of the crack tip.

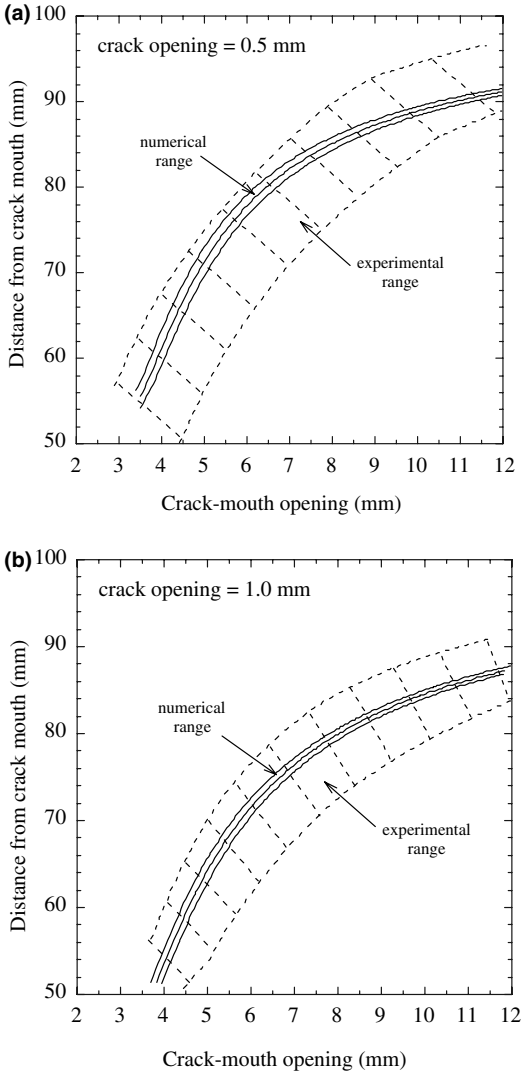

Fig. 12. Plots of how the distance from the crack mouth at which the crack-opening displacement is (a) 0.5 mm, and (b) 1.0 mm, varies with the opening of the crack mouth. Comparisons are shown between the experimentally observed range (shown shaded) and the range predicted from the CZM parameters, given the uncertainties in the cohesive parameters.

The values of the cohesive-zone parameters for the composite can further be confirmed by looking at how the crack and bridged region evolve upon loading. The cohesive-zone parameters would indicate a critical crack opening at which fiber-pull-out is complete of 1.0 ± 0.2 mm. While this number is certainly in a range that is consistent with experimental observations of the crack-tip region (Fig. 10), in practice there is a range of pull-out lengths and no clear boundary between the bridged and unbridged crack. Therefore, an alternative approach to verify the cohesive-zone parameters is to look at the crack opening within the bridged zone. This was done by monitoring how the point at which the crack opening had a specified value moved as the specimen was loaded. Specifically, a scale was fixed to the surface of a compact-tension specimen that allowed the distance of this point from the crack mouth to be measured (Fig. 11). A CCD camera was used to record images of the bridged region of the crack. As the load increased and the crack advanced, these images were used to determine the distance from the crack mouth where the opening-displacement was equal to 1.0 and 0.5 mm. This distance was then plotted as a function of the opening-displacement of the crack mouth (which is related to the applied load – see Fig. 7). Numerical analyses were performed for the geometry using the cohesive-zone model, and the results were used to calculate the distance from the crack mouth at which the crack opening reached 1.0 and 0.5 mm as a function of opening-displacement of the crack mouth. A comparison between the experimental data and the numerical predictions are shown in Fig. 12. While there is a fairly large range of experimental uncertainty, associated with the difficulty of measuring the crack opening precisely, the numerical predictions lie well within the experimental band, supporting the values of the cohesive-zone parameters deduced for this composite.

4. Discussion

4.1. Three-parameter cohesive zone model

A two-parameter cohesive-zone model with a toughness and a single characteristic strength describes the fracture behavior of cracked geometries such as the compact-tension specimen very well (Fig. 9). However, an inconsistency can immediately be seen when the results of the tensile tests are considered. In these tests, fracture occurred at tensile stresses between 80 and 120 MPa, which is a significantly higher range than that deduced for the characteristic strength (71–87 MPa). This indicates that the cohesive strength of the composite must actually be larger than the value deduced for the characteristic strength, but simple cohesive laws with characteristic strengths in the range of 80–120 MPa do not result in satisfactory predictions for the behavior of the compact-tension tests.

This apparent paradox can be resolved by assuming that the fracture process involves two completely separate processes: matrix cracking followed by fiber pull-out, with the toughness contribution coming primarily from the fiber pull-out. Such a phenomenon is consistent with the physics of composite failure, and was illustrated schematically in Fig. 2. In that figure, the matrix-cracking strength was drawn as being less than the bridging strength; however, the data for this composite indicate that the matrix-cracking strength is bigger than the bridging strength. Therefore, when the characteristic dimensions (crack or ligament size) of a specimen become very small, failure is dominated by the matrix

strength, rather than by the bridging strength, which remains the characteristic strength associated with toughening by fiber pull-out. It should be noted that the strength of the fibers may be limited by frictional pull-out, or by an actual fracture strength. Furthermore, the matrix-cracking strength includes both the stress supported by the matrix and the stress supported by the fibers, while the bridging strength is the maximum load supported by the fibers averaged over the cracked area. The two strengths can either be determined by experimental observations, as done in this paper, or by micro-mechanics modeling if the appropriate parameters are known.

A simple cohesive law that can easily be implemented in numerical calculations, and that captures the concepts of matrix cracking and fiber pull-out is shown in Fig. 13. The total area under the cohesive law was set at $\Gamma = 40 \pm 4$ kJ m^{-2}, with a fiber pull-out strength of $\hat{\sigma}_b = 79 \pm 8$ MPa (the characteristic strength from the compact tension tests). The matrix-cracking strength, $\hat{\sigma}_m$, was set at 100 ± 20 MPa, based on the uniaxial tensile tests. This choice is a lower bound that probably amalgamates the fracture parameters of the matrix with the effects of inhomogeneties within the composite. It has the advantage of numerical simplicity, in that intrinsic flaws do not need to be modeled when analyzing the behavior of nominally uncracked composites. If the intent were to model accurately the details of matrix cracking, a more sophisticated analysis of the matrix-cracking strength would be needed. However, the intent here is to provide predictions of the macroscopic behavior of the composite from a design perspective, and the approach used appears to serve this purpose very well. The remaining details of the curve, i.e., the displacements corresponding to $\hat{\sigma}_b$ and $\hat{\sigma}_m$, were chosen so as to mimic the initial elastic behavior of the composite followed by a relatively sudden drop in strength that would not cause numerical difficulties. When this three-parameter cohesive-zone model was used to compute the behavior of the compact-tension specimen, the results were indistinguishable from the results based on the two-parameter model, already plotted in Figs. 9 and 12. However, the three-parameter model also successfully described the behavior of the tensile specimens shown in Fig. 5(a). The additional cohesive-strength parameter for this material is required when analyzing geometries with very small crack or ligament lengths.

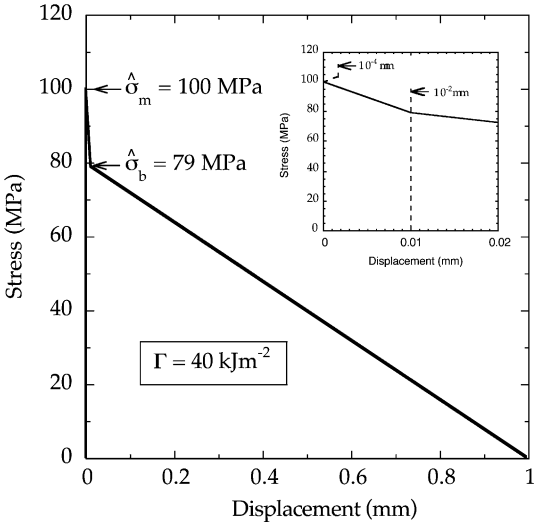

Fig. 13. Schematic traction–separation law used to describe the fracture of this composite. The peak load corresponds to matrix cracking. This is followed by fiber pull-out.

4.2. Single-edge notched tensile specimens

As noted above, the results of numerical calculations for cracked geometries are unaffected by the introduction of a second strength parameter, but the three-parameter model gives correct predictions for the behavior of the tensile specimen, predicting catastrophic failure at the peak load with no crack growth. However, since the uncracked tensile specimen was actually used to deduce $\hat{\sigma}_b$, as described in the previous section, a different geometry was required to test whether the cohesive-zone model could be used in a predictive fashion. Therefore, numerical and experimental studies were conducted on a series of single-edge-notched tension (SENT) specimens with a width $w = 25 \pm 0.5$ mm, a length $L = 140 \pm 2$ mm, a thickness $t = 2.8 \pm 0.1$ mm, and various initial notch depths (Fig. 14).

The numerical studies were done by applying fixed-displacement boundary conditions to the ends of the specimen, and the tensile behavior was predicted as a function of initial notch size using the three-parameter cohesive-zone model of Fig. 13. A plot of how the average ligament strength (maximum load normalized by ligament area) is predicted to vary with notch length is shown in Fig. 15. Superimposed on this plot are experimental results for the strength obtained by gripping

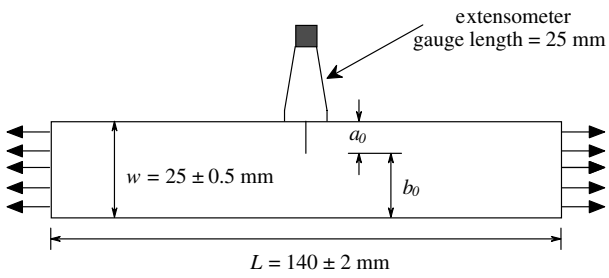

Fig. 14. The geometry of the single-edge notched tensile (SENT) specimens used in this study. In the experimental tests, the ends of the specimen were supported by wedge grips. Constant displacement conditions were applied to the ends of the specimens in the numerical simulations. The thickness of the specimens was $t = 2.8 \pm 0.1$ mm.

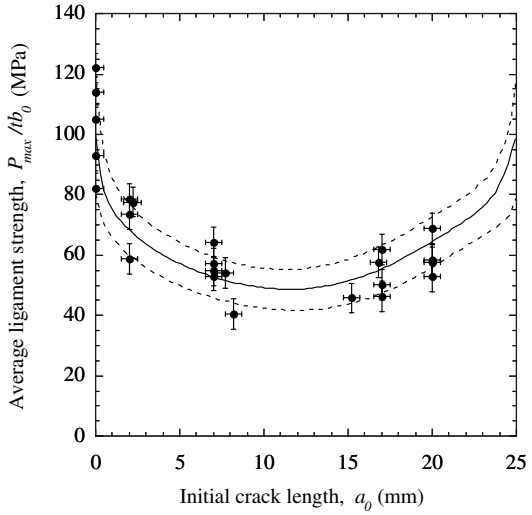

Fig. 15. Plots of the average strength of the ligament against initial notch length for the single-edge-notched tensile specimens shown in Fig. 14. The solid line represents the numerical predictions, while the dashed lines indicate the range of uncertainty for these predictions. The uncertainties are associated with the uncertainties for the modulus of the composite and for the cohesive parameters. The experimental data are represented as points to show a comparison with the numerical predictions.

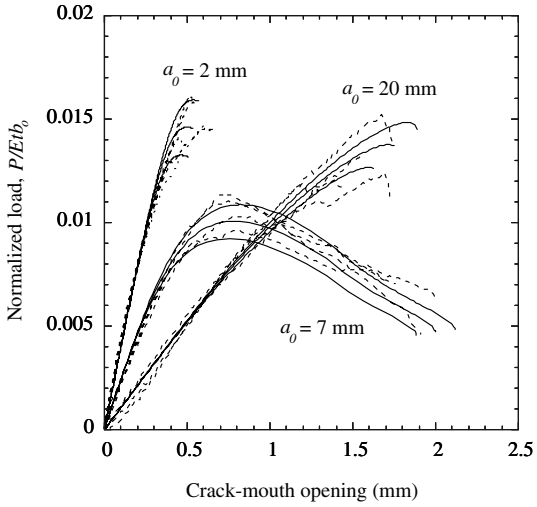

Fig. 16. Plots of normalized average stress acting on the ligament (P/Etb_0) against the opening of the notch mouth for single-edge-notched tensile specimens with initial notch sizes of $a_0 = 2$, 7 and 20 mm. These plots show comparisons between the predictions of a cohesive-zone model and the experimental results. The solid curves represent the numerical data and the dotted lines represent the experimental data. The range in the numerical results indicates the effects of uncertainty in the cohesive parameters, geometrical parameters and the modulus.

the specimen in wedge grips, and testing at a displacement rate of 0.01 mm s^{-1}. Of particular note in the numerical predictions is that when the characteristic dimension of the specimens (either the notch or ligament size) is very small, the ligament strength is controlled by the cohesive strength of the composite (the matrix-cracking strength in this case). With a larger characteristic dimension, both the toughness and associated characteristic strength (the fiber-bridging strength) control the strength of the composite. The effect of uncertainty in the matrix strength can be seen in this figure – it affects the average ligament strength only when the specimen has very small characteristic dimensions. At larger dimensions, the uncertainty in the strength is dominated by the uncertainty in the toughness and in the characteristic strength. The experimental results follow the predicted trends in strength.

Comparisons between the numerical predictions for the load versus crack-mouth opening displacements and the experimental results with different initial notch lengths are shown in Fig. 16. Of particular note is that, not only are the peak loads correctly predicted, but the numerical calculations also predict the onset of catastrophic failure for each set of specimens and, hence, the maximum applied displacement. The specimens with an initial notch of 2 mm exhibited catastrophic failure with no observable crack growth. The specimens with an initial notch of 7 mm exhibited some crack growth before failing catastrophically, while the specimens with an initial notch of 20 mm failed catastrophically with no observed crack growth. It should be noted that essentially identical results are obtained for the two-parameter and three-parameter models for these three notch sizes, since the size of the notch or ligament are too large for the behavior of the specimen to be significantly affected by the matrix strength.

4.3. Transition to catastrophic failure and energy dissipation during fracture

Both the experimental and numerical results described in the previous section exhibited transitions between stable cracking and catastrophic failure. Cox and Marshall [13] explored the effects of transitions in the length of the bridging zone on the ductile-to-brittle transition in composites. However, in the present situation, the steady-state cohesive-zone length is fixed, because the toughness has been defined as being constant. An alternative mechanism for the transition to unstable fracture can occur automatically if a crack is sufficiently small that the stress required to propagate it is greater than the maximum bridging strength [4,8,24]. Load-control is a common analytical assumption, and the conditions for catastrophic failure can readily be found by identifying the maximum load required to propagate a crack. However, in many practical situations, the load is applied under displacement-controlled conditions. Under these conditions, an instability occurs when the force is decreasing and the derivative of the applied displacement with respect to the resultant force, $d\Delta/dF$, equals zero. This corresponds

to the condition when there is enough elastic energy for the crack to propagate with no additional work being done by the applied loads, and results in a transition to dynamic fracture. Cohesive-zone models are easily analyzed under displacement-control, and this condition of $d\Delta/dF = 0$ can easily be determined to identify the onset of catastrophic failure. [5] However, a further discussion of how these instabilities are linked to the total energy dissipated by a composite upon fracturing into two parts is quite illuminating.

Fig. 17(a) shows a plot of the total energy dissipated per unit width (defined and measured as the area under the load–displacement curve up to the maximum displacement when the system separates into two parts) as a function of the initial notch size during fracture of the SENT geometry shown in Fig. 14. Fig. 17(b) shows the same data as Fig. 17(a), but with the energy normalized by the ligament area. Four distinct regions are identified in Fig. 17(a) and (b). (i) An unstable region when the initial crack is very small, where the transition to catastrophic failure occurs before the full development of a cohesive zone. (ii) A region at intermediate crack sizes in which the crack grows with a fully developed cohesive zone ahead of it. (iii) A second unstable region in which catastrophic crack growth occurs because the cohesive-zone interacts with the free boundary before a steady-state configuration is reached. All cracks that start off growing in the intermediate stable region grow to the same critical length before a transition to catastrophic growth occurs. (iv) A final stable regime that is observed when the initial ligament is short enough for the cohesive zone to extend all the way across the ligament and for the fracture load to be sufficiently low that the composite surfaces move apart in a stable manner until complete separation occurs. The boundaries between these regimes depend on the properties of the composite, and on details of the loading and geometry. For example, shorter specimens that are loaded by rigid grips will tend to have larger regimes of stability. However, the existence of these different regions of stability is expected to be a general phenomenon, and the physics of the transitions between the regions is discussed in more detail below.

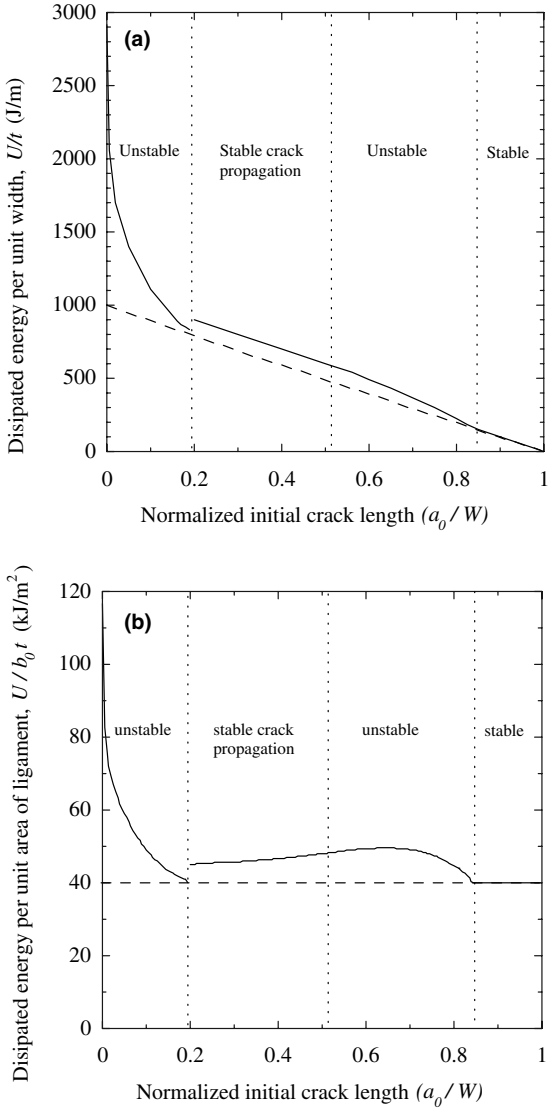

Fig. 17. Predictions of how (a) the total energy dissipated per unit width and (b) the total energy dissipated per unit initial ligament area vary as a function of initial crack length for the SENT specimens with the geometry shown in Fig. 14. The dotted line indicates the value of the characteristic toughness used in these calculations, $\Gamma = 40\ \mathrm{kJ\,m^{-2}}$. Other values of the material properties used for these calculations are: $E = 6.0$ GPa, $\hat{\sigma}_m$=100 MPa, and $\hat{\sigma}_b$=79 MPa. The major experimental uncertainties in this plot arise from the measurement of the crack and ligament length.

The energy dissipated during fracture of an elastic material under displacement control is the work done by the applied loads up to the maximum displacement. It consists of two parts: (i) the energy associated with creating two new surfaces during loading, (ii) the elastic energy stored in the system at any transition to instability upon the onset of catastrophic crack propagation. The first term includes the energy associated with the partial creation of a fracture surface ahead of the crack tip (in the cohesive zone), and the surface energy associated with any stable crack growth prior to the onset of

[5] The numerical calculations in this paper were static calculations that terminated at the onset of a numerical instability. However, numerical algorithms to ensure stability, such as Riks method [1], showed that these conventional analyses broke down only when $d\Delta/dF = 0$, and that there was no subsequent stable regime for these geometries. Similar observations that the numerical instabilities can be identified with physical instabilities in the real system have been made in related cohesive-zone studies [17,48,49]. Other numerical instabilities caused by mesh size or the shape of the traction–separation law do not have a physical basis, and have been separated from the effect being discussed here. All instabilities discussed in this paper have a physical meaning, and are not numerical artifacts.

instability. The second term is converted to kinetic energy and to whatever surface energy remains to be created upon final separation of the material. [6] The total dissipated energy cannot be less than the fracture energy $\Gamma b_0 t$ (represented by the dashed line in Fig. 17), where b_0 is the initial ligament length and t is the thickness of the composite. However, even in a perfectly elastic system, the total dissipated energy can be greater than the fracture energy because elastic energy is lost in the form of kinetic energy or phonon emission when a crack propagates under non-equilibrium conditions. When the initial notch is small, the instability condition is satisfied before a fully developed cohesive zone is established. As the initial notch size increases, the work required to develop a cohesive zone ahead of the crack decreases more rapidly than the energy required to rupture the remaining ligament. The length of the cohesive zone at the point of instability increases and, eventually, a fully developed cohesive zone is just established at the point of instability. This is the transition condition for the crack to begin growing in a stable manner with a steady-state cohesive zone ahead of the tip; it appears to correspond to the situation when there is just enough elastic energy stored in the composite to separate the remaining ligament spontaneously. [7] This condition, defining the boundary between the unstable regime and the regime in which steady-state crack growth occurs, appears to be a general requirement for the onset of stability. This point can be appreciated more fully by examination of Fig. 17. It should be noted that the size of the critical notch at which the transition between stable and unstable growth occurs depends on the length of the specimen, but the condition that the work done to create a fully developed cohesive zone be approximately equal to the energy required to rupture the remaining ligament is always maintained.

The rate of decrease of energy dissipation with ligament area must always equal Γ during stable crack growth. This proportionality can be seen in Fig. 17. However, it will be noted that, in this case, additional work is done on the composite above that required to separate the ligament. This excess energy manifests itself by the onset of a second regime of instability, after the crack has grown for some length and the cohesive zone interacts with the free surface. It is this second regime of instability that limits the length of stable crack growth. No matter what the initial notch length is, a stable crack always grows to the same point before the instability occurs. If the geometry was such that there was no second instability, the total energy dissipated would follow the minimum line given by $\Gamma b_0 t$ all the way from the start of the stable crack regime to zero ligament thickness. If the initial ligament is short enough, there will always be a final regime of complete stability in which the applied loads drops smoothly to zero as the surfaces separate, so the total work done is equal to the toughness times the ligament area. The size of initial ligament length for which this regime can be obtained depends on the compliance of the composite – as before, shorter lengths of composite will enhance the stability of fracture.

The stability behavior described above is essentially identical to what would be obtained with a two-parameter cohesive law, except for the details at extremely small crack and ligament sizes (less than about half a millimeter). A similar discussion on stabilities and energy dissipation is expected to be pertinent for understanding the behavior of Izod and Charpy tests; cohesive zone modeling with appropriate rate-dependent properties could probably be used to provide predictive analyses of these tests. [8]

5. Conclusions

Cohesive-zone models provide a useful design tool for predicting the fracture of fiber-reinforced polymer–matrix composites. A characteristic toughness and a characteristic strength appear to suffice generally for describing the behavior of cracked bodies. However, while any generic two-parameter cohesive law provides adequate predictive capabilities for many purposes, extra details of the law (such as the shape) may sometimes be required for accurate modeling when the characteristic dimensions of a specimen are very small. In the present case, the effect of including matrix cracking in the analysis was discussed. Appropriate values for the cohesive parameters can be determined by comparing the results of suitable experiments to numerical calculations. Once these parameters have been determined, general load–displacement curves can be computed for different geometries that give good predictions for the performance of the composite, including strengths, compliances and energy dissipation. In particular, the approach appears to predict accurately the onset of catastrophic failure in static tests – a mode of fracture in which the crack makes a

[6] Stored elastic energy is recovered and converted to fracture energy during stable crack growth under equilibrium conditions.

[7] Since the elastic displacements associated with the composite are much greater than the displacements associated with the cohesive zone, the work done by the applied loads is essentially identical to this value of stored strain energy.

[8] If a lower-toughness mode of crack growth exists, then switching to this mode may precipitate catastrophic failure earlier than predicted by the static analysis. Studies of this material in the authors' laboratory [41] suggest that it is not very rate sensitive, and this model for the transition to dynamic fracture may be appropriate.

transition to a dynamic mode, causing rupture with no further input of energy into the system.

Acknowledgements

S.L., M.D.T. and A.M.W. gratefully acknowledge the financial support of General Motors. All the authors gratefully acknowledge the supply of the composite from Azdel, Inc. We also thank a reviewer of this article for a very detailed and careful review of the original manuscript.

References

[1] ABAQUS Finite Element Analysis Code and Technical Manual, Version 6.2, Hibbit, Karlsson and Sorensen Inc., 2001.
[2] ASME D5379/D5379M-98, Standard test method for shear properties of composite materials by the V-notched beam method, American Society for Testing and Materials, West Conshohocken (PA), 1999.
[3] Aveston J, Cooper GA, Kelly A. Single and multiple fracture. In: The properties of fibre composites. Science and Technology Press Ltd; 1971. p. 15–24.
[4] Bao G, Suo Z. Remarks on crack bridging concepts. Appl Mech Rev 1992;45:355–66.
[5] Bilby BA, Cottrell AH, Swinden KH. The spread of plastic yielding from a notch. Proc Royal Soc A 1963;272:304–14.
[6] Barenblatt GI. The mathematical theory of equilibrium of cracks in brittle fracture. Adv Appl Mech 1962;7:55–129.
[7] Budiansky B. Micromechanics II. In: Proceedings of the 10th US National Congress of Applied Mechanics, Austin, TX, 1986. p. 25–32.
[8] Cox BN. Extrinsic factors in the mechanics of bridged cracks. Acta Metall Mater 1991;39:1189–201.
[9] Cox BN. Scaling for bridged cracks. Mech Mater 1993;15:87–98.
[10] Cox BN, Dadkhah MS, Morris WL. On the tensile failure of 3-D woven composites. Composites A 1996;27:447–58.
[11] Cox BN, Lo CS. Load ratio, notch, and scale effects for bridged cracks in fibrous composites. Acta Metall Mater 1992;40:69–80.
[12] Cox BN, Marshall DB. The determination of crack bridging forces. Int J Fract 1991;49:159–76.
[13] Cox BN, Marshall DB. Stable and unstable solutions for bridged cracks in various specimens. Acta Metall Mater 1991;39:579–89.
[14] Cox BN, Marshall DB, Thouless MD. Influence of statistical fiber strength distribution on matrix cracking in fiber composites. Acta Metall Mater 1989;37:1933–43.
[15] Dugdale DS. Yielding of steel sheets containing slits. J Mech Phys Solids 1960;8:100–8.
[16] Hinton MJ, Kaddour AS, Soden PD. A comparison of the predictive capabilities of current failure theories for composite laminates, judged against experimental evidence. Compos Sci Technol 2002;62:1725–97.
[17] Kafkalidis MS, Thouless MD. The effects of geometry and material properties on the fracture of single lap-shear joints. Int J Solids Struct 2002;39:4367–83.
[18] Leung CK, Li VC. Effects of fiber inclination on crack bridging stresses in fiber reinforced brittle matrix composites. J Mech Phys Solids 1992;40:1333–62.
[19] Li S. Fracture analysis of an adhesively-bonded polymer–matrix composite, PhD dissertation, University of Michigan, Ann Arbor, MI, 2004.
[20] Li S, Wang J, Thouless MD. The effects of shear on delamination in layered materials. J Mech Phys Solids 2004;52:193–214.
[21] Li S, Thouless MD, Waas AM, Schroeder JA, Zavattieri PD. Analyzing mode-I fracture of an adhesively-bonded polymer–matrix composite using a cohesive-zone model. J Compos Sci Technol, in press.
[22] Li S, Thouless MD, Waas AM, Schroeder JA, Zavattieri PD. Mixed-mode cohesive-zone models for fracture of an adhesively-bonded polymer–matrix composite, submitted for publication.
[23] Li VC, Chan CM, Leung CKY. Experimental determination of the tension-softening relations for cementitious composites. Cem Concr Res 1987;17:441–52.
[24] Li VC, Leung CKY. Steady state and multiple cracking of short random fiber composites. ASCE J Eng Mech 1992;118: 2246–2264.
[25] Li VC, Maalej M, Hashida T. Experimental determination of the stress-crack opening relation in fibre cementitious composites with a crack-tip singularity. J Mater Sci 1994;29:2719–24.
[26] Li VC, Wang Y, Backer S. Effect of inclining angle, bundling and surface treatment on synthetic fiber pull-out from a cement matrix. Composites 1990;21:132–40.
[27] Li VC, Ward RJ. A novel testing technique for post-peak tensile behavior of cementitious materials. In: Mihashi H, Takahashi FH, Wittmann AA, editors. Fracture toughness and fracture energy – testing methods for concrete and rocks. Rotterdam: Balkema; 1989. p. 183–95.
[28] Lindhagen JE, Berglund LA. Application of bridging-law concepts to short-fibre composites. Part 1: DCB test procedures for bridging law and fracture energy. Compos Sci Technol 2000;60:871–83.
[29] Lindhagen JE, Berglund LA. Application of bridging-law concepts to short-fibre composites. Part 2: Notch sensitivity. Compos Sci Technol 2000;60:885–93.
[30] Lindhagen JE, Gamstedt EK, Berglund LA. Application of bridging-law concepts to short-fibre composites. Part 3: Bridging law derivation from experimental profiles. Compos Sci Technol 2000;60:2883–94.
[31] Marshall DB, Cox BN, Evans AG. The mechanics of matrix cracking in brittle matrix composites. Acta Metall 1985;33:2013–21.
[32] McCartney LN. Mechanics of matrix cracking in brittle-matrix fibre-reinforced composites. Proc Royal Soc A 1987;409:329–50.
[33] Needleman A. A continuum model for void nucleation by inclusion debonding. J Appl Mech 1987;54:525–31.
[34] Rice JR. Mathematical analysis in the mechanics of fracture. In: Sih GC, editor. Fracture: an advanced treatise, vol. 2. New York: Academic Press; 1968. p. 191.
[35] Rose LRF. Crack reinforcement by distributed springs. J Mech Phys Solids 1987;35:383–405.
[36] Shahwan K, Waas AM. Non-self-similar decohesion along a finite interface of unilaterally constrained delaminations. Proc Royal Soc A 1997;453:515–50.
[37] Song SJ, Waas AM. Modeling crack growth in laminates via a novel strength criterion. ASME Trans, J Eng Mater Technol 1994;116:512–6.
[38] Song SJ, Waas AM. An energy based model for mixed mode failure of laminated composites. AIAA J 1995;33:739–45.
[39] Sørensen BF, Jacobsen TK. Large-scale bridging in composites: *R*-curves and bridging laws. Composites A 1998;29: 1443–1451.
[40] Sørensen BF, Jacobsen TK. Determination of cohesive laws by the *J* integral approach. Eng Fract Mech 2003;70:1841–58.
[41] Sun C. unpublished work, 2003.
[42] Suo Z, Ho S, Gong X. Notch ductile-to-brittle transition due to localized inelastic band. J Eng Mater Technol 1993;115:319–26.
[43] Thouless MD. Bridging and damage zones in crack growth. J Am Ceram Soc 1988;71:408–13.

[44] Thouless MD. A re-examination of the analysis of toughening in brittle-matrix composites. Acta Metall 1989;37:2297–304.
[45] Thouless MD, Evans AG. Effects of pull-out on the mechanical properties of ceramic-matrix composite. Acta Metall 1988;36:517–22.
[46] Tvergaard V, Hutchinson JW. The relation between crack growth resistance and fracture parameters in elastic–plastic solids. J Mech Phys Solids 1992;40:1377–97.
[47] Ungsuwarungsri T, Knauss WG. Role of damage-softened material behavior in the fracture of composites and adhesives. Int J Fract 1987;35:221–41.
[48] Yang QD, Thouless MD. Mixed-mode fracture analyses of plastically-deforming adhesive joints. Int J Fract 2001;110:175–87.
[49] Yang QD, Thouless MD, Ward SM. Numerical simulations of adhesively-bonded beams failing with extensive plastic deformation. J Mech Phys Solids 1999;47:1337–53.